Structural stability of silica at high pressures and temperatures

Artem R. Oganov,[1,*] Michael J. Gillan,[2] and G. David Price[2]
[1]*Laboratory of Crystallography, Department of Materials, ETH Hönggerberg, HCI G515, Wolfgang-Pauli-Strasse 10, Zurich CH-8093, Switzerland*
[2]*University College London, Gower Street, London WC1E 6BT, United Kingdom*
(Received 11 October 2004; published 17 February 2005)

The high-pressure phase diagram of SiO_2 has been calculated using density-functional perturbation theory. We find that phase transitions of silica do not correspond to any observed seismic discontinuities within the Earth. We analyze the breakdown of close packing occurring in SiO_2 above 200 GPa and conclude that it is due to asphericity and deformability of ions, which can generally lead to the formation on non-close-packed structures at high pressure. Our calculations indicate that pyrite-structured SiO_2, stable above 200 GPa, has no soft modes down to ambient pressure and could, therefore, be quenchable. Above 750 GPa a cotunnite-type phase is stable.

DOI: 10.1103/PhysRevB.71.064104 PACS number(s): 61.50.Ks, 61.50.Ah, 64.70.Kb, 65.40.Gr

I. INTRODUCTION

Silica (SiO_2) polymorphs are of great importance in solid state physics, technology, and Earth sciences. Understanding their high-pressure behavior can provide many useful ideas—especially for crystal chemistry of silicates that make up most of the Earth's mantle. For example, the discovery of stishovite, a rutile-structured silica polymorph[1] [Fig. 1(a)], has revolutionized the understanding of the deep Earth's interior by suggesting that in deep-mantle silicates Si atoms are octahedrally (rather than tetrahedrally) coordinated. The transition from the fourfold to sixfold coordination, at least in liquids, may proceed via an intermediate exotic fivefold coordination.[2,3] Many years after the discovery of stishovite, two post-stishovite phases were identified: those with the $CaCl_2$-type structures [which for brevity we denote here as SiO_2-I, Fig. 1(b) and α-PbO_2-type (SiO_2-II, Fig. 1(c)]; theoretical studies suggested that at still higher pressures a pyrite-type phase [SiO_2-III, Fig. 1(c)] is stable. The pressure-temperature stability fields of these phases remain poorly known.

It is well established[4–10] that at ~50 GPa and 298 K stishovite undergoes a second-order transition to SiO_2-I, although recently this transition was argued to be first order due to strain-order parameter coupling.[11] This transition was proposed[5,12] as the cause of the seismic anomaly observed in the Earth at the depth of 1200 km. Above ~90 GPa an α-PbO_2 structured phase (SiO_2-II) becomes stable, having space group *Pbcn* (Refs. 6 and 7) or its polar subgroup *Pnc*2.[8,13]

The structures of stishovite SiO_2-I and SiO_2-II are based on the hexagonal close packing of oxygens with Si atoms filling half of the octahedral voids; there are many energetically similar metastable structures[7] differing only in the distribution of cations over the octahedral voids. At high temperatures a disordered distribution is possible—as in the Fe_2N-type structure, experimentally found to be metastable for SiO_2 (Ref. 14).

According to theory,[6–8] SiO_2-II is stable up to ~200 GPa, when it transforms to a pyrite-type phase (SiO_2-III). Silica has not yet been studied experimentally at conditions appropriate for synthesis of SiO_2-III, but pyrite-type phases are known for analogous materials at high pressure: RuO_2, PbO_2, GeO_2 (Ref. 15), and SnO_2 (Ref. 16). The pyrite structure (SiO_2-III) marks a new twist in structural chemistry of silica: it is not close packed, yet much denser than close-packed structures of stishovite, SiO_2-I, and SiO_2-II. Two additional features make this structure especially interesting: unusual 6+2 coordination of Si, and relatively short O-O contacts with a possibility of O-O bonds. Indeed, typical pyrites MX_2 do have *X*-*X* covalent bonds. Here we focus on two issues: (1) high-pressure phase diagram of SiO_2 and its geophysical significance and (2) investigation of the pressure-induced breakdown of structural close packing associated with the formation of SiO_2-III.

II. COMPUTATIONAL METHODOLOGY

Our calculations are based on density-functional perturbation theory (for a review, see Ref. 17) within the local density approximation[18] (LDA) and pseudopotential plane wave method as implemented in the ABINIT code.[19] We used nonlocal Troullier-Martins pseudopotentials[20] with partial core corrections[21] and plane wave basis sets with a 40 Ha cutoff. The pseudopotential core radii are 0.766 Å for O ($1s^2$ core) and 1.105 Å for Si ($1s^2 2s^2 2p^6$ core). The Brillouin zone was sampled with $4\times4\times6$ (for stishovite and SiO_2-I) and $4\times4\times4$ (for SiO_2-II and SiO_2-III) Monkhorst-Pack meshes. Electronic self-consistency was performed until forces converged to within 10^{-6} Ha/Bohr; crystal structures were optimized by steepest descent until forces on atoms were below 10^{-5} Ha/Bohr. With our computational settings, the total energies, energy differences between polymorphs, pressure, and phonon frequencies are converged to within 14×10^{-3} eV/atom, 2×10^{-3} eV/atom, 0.3 GPa, and 1 cm^{-1}, respectively. Dynamical matrices were calculated on a $2\times2\times3$ (stishovite and SiO_2-I) and $2\times2\times2$ (SiO_2-II and SiO_2-III) grids and then interpolated throughout the Brillouin zone using the technique,[22] explicitly accounting for the long-range electrostatic contributions. The interpolation er-

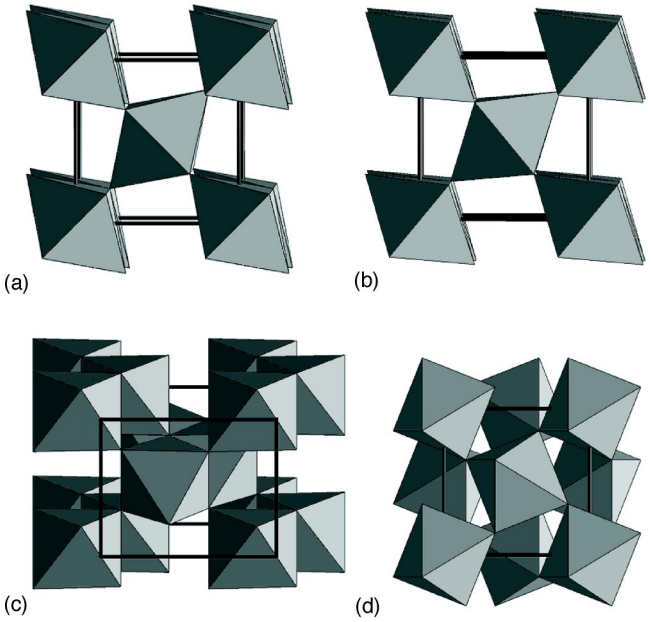

FIG. 1. Calculated structures of SiO_2 phases. (a) stishovite at 20 GPa, (b) SiO_2-I at 70 GPa, (c) SiO_2-II at 120 GPa, (d) SiO_2-III at 220 GPa.

rors are within 12 cm^{-1} in stishovite and SiO_2-I, and within 5 cm^{-1} in SiO_2-II and SiO_2-III.

Our calculations clearly confirm the second-order nature of the stishovite-(SiO_2-I) transition with mechanical instability ($C_{11}-C_{12}=0$) precisely (within 1 GPa) at the thermodynamic transition pressure, and we see no hysteresis in this transition. For SiO_2-II we find that the true symmetry is *Pbcn*: starting with a distorted *Pnc*2 structure we obtained *Pbcn* after structural optimisation, in agreement with findings of Ref. 7. We note that the *Pbcn* structure has no soft modes.

Diagonalizing the dynamical matrices at a large number of wave vectors, we obtain the phonon density of states $g(\omega)$ and can evaluate thermodynamic functions, e.g., heat capacity C_V, entropy S, and Helmholtz free energy F, as a function of temperature:

$$C_V(T) = k_B \int_0^{\omega_{\max}} \left(\frac{\hbar\omega}{k_B T}\right)^2 \frac{\exp\left(\frac{\hbar\omega}{k_B T}\right)}{\left[\exp\left(\frac{\hbar\omega}{k_B T}\right)-1\right]^2} g(\omega)d\omega, \tag{1}$$

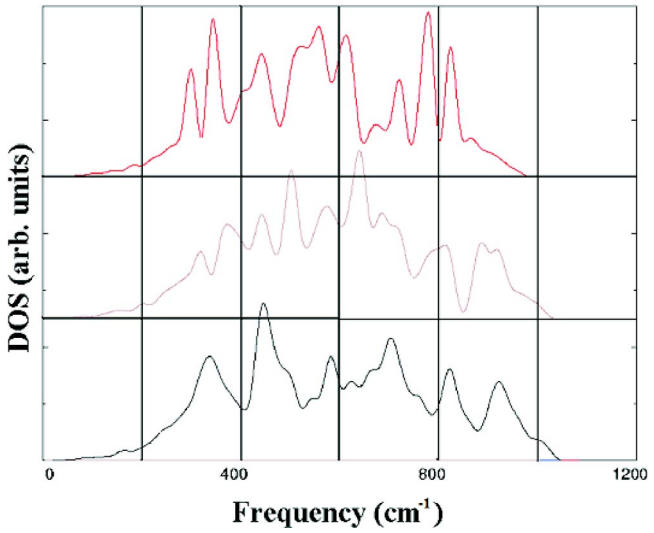

FIG. 2. (Color online) Calculated phonon densities of states of stishovite (bottom), SiO_2-II (middle) and SiO_2-III (top) at $P=0$.

$$S(T) = \int_0^{\omega_{\max}} \left\{ -k_B \ln\left[1-\exp\left(-\frac{\hbar\omega}{k_B T}\right)\right] + \frac{1}{T}\frac{\hbar\omega}{\exp\left(\frac{\hbar\omega}{k_B T}\right)-1} \right\} g(\omega)d\omega, \tag{2}$$

$$F(T) = E_0 + \int_0^{\omega_{\max}} \left\{ \frac{\hbar\omega}{2} + k_B T \ln\left[1-\exp\left(-\frac{\hbar\omega}{k_B T}\right)\right] \right\} g(\omega)d\omega, \tag{3}$$

where E_0 is the energy of the static lattice, $\hbar$ the Planck constant, and k_B the Boltzmann constant. Examples of calculated phonon densities of states are given in Fig. 2. As Table I shows, such calculations are able to reproduce experimental data for SiO_2 and other materials rather accurately.

Within the quasiharmonic approximation, we have explored both thermodynamic and dynamical stability of SiO_2 polymorphs; mechanical stability was studied separately by calculating the elastic constants from nonlinear stress-strain relations. We calculate the Gibbs free energy via the Helm-

TABLE I. Thermodynamic properties ($J\,mol^{-1}\,K^{-1}$) of phases in the MgO-SiO_2 system: theory and experiment (0 GPa, 300 K).

	MgO Periclase		SiO_2 Stishovite		SiO_2-II	SiO_2-III	$MgSiO_3$ Perovskite	
	theory (Ref. 23)	exp (Ref. 24)	theory	exp (Ref. 25)	theory	theory	theory(Ref. 26)	exp (Ref. 27)
C_V	36.58	36.87	41.3[a]	42.2	41.1[a]	42.5[a]	80.73	77.3
S	26.81	27.13	24.6[a]	25.9	23.7[a]	24.9[a]	57.14	57.2

[a]This work.

TABLE II. Static equations of state. SiO_2-I is unquenchable, its zero-pressure properties are only fitted parameters. Total energy and volume (values per formula unit), bulk modulus and its pressure derivative are given.

Phase	E_0, a.u.	V_0, Å^3	K_0, GPa	K_0'
Stishovite[a]	−37.7979568	23.1559	318.326	4.3726
SiO_2-I	(−37.7996067)	(23.5751)	(258.354)	(4.6135)
SiO_2-II	−37.7925485	22.7805	324.426	4.2327
SiO_2-III	−37.7597881	21.7481	344.806	4.3130

[a]Third-order Birch-Murnaghan equation of state from experiment (Ref. 9): V_0=23.315 Å^3, K_0=291 GPa, K_0'=4.29.

holtz free energy obtained directly in our calculations $G(P,V)=F(V,T)+PV$, where

$$P=-\left(\frac{\partial F}{\partial V}\right)_T$$

The static part of $F(V,T)$ was represented by the Vinet equation of state[28] (Table II), the vibrational part was well fitted by third-order polynomial functions of volume at each temperature. Since the stishovite-(SiO_2-I) phase transition is due to the onset of a mechanical instability of stishovite, the corresponding phase equilibrium line was found as a set of P,T points at which stishovite becomes mechanically unstable. All other equilibrium lines were found by examining free energy differences. Methodology used here is very similar to that of our recent works.[23,26,29]

For the analysis of chemical bonding in SiO_2 polymorhps we employ topological analysis of electron density,[30] electron localization function,[31] and localized orbital locator.[32] For topological analysis, the total density was restored by adding atomic core electron density to the valence density obtained in our pseudopotential calculations. As shown by Bader,[30] the total electron density can be uniquely partitioned into atomic basins with well-defined, additive, and transferable properties, such as atomic volumes and charges. There are different types of critical points at boundaries between atomic basins; $(3,-1)$ points can be used to define atomic coordination. The density Laplacian ($\nabla^2\rho$) indicates regions of electronic concentration ($\nabla^2\rho<0$) or depletion ($\nabla^2\rho>0$); $\nabla^2\rho<0$ in the bonding region shows a shared (covalent) interaction as opposed to closed-shell interactions. Our calculations suggest that chemical bonding in stishovite and phases I–III is similar: at all pressures studied here these phases are wide-gap insulators, predominantly ionic with a covalent component for Si-O bonds (see also Bader and Born atomic charges in Table III), Si in the octahedral coordination, and similar parameters of Si-O bond critical points. The six $(3,-1)$ bond critical points between Si and O in SiO_2-III are characterized by low electron density (0.70e Å^{-3} at zero pressure) and positive Laplacian $\nabla^2\rho$ (8.12e Å^{-5}), suggesting that Si-O interaction is closed shell. From atomic volumes (Table III) we see that crystal volume is dominated by O atoms.

TABLE III. Bader volumes and charges at 0 GPa. For comparison, tetrahedral Si in sillimanite (Al_2SiO_5) has Z_{Si}=3.164 (3.191) $|e|$, V_{Si}=3.223 Å^3.

Phase	Z_{Si}, $\|e\|$	V_{Si}, Å^3	Z_O, $\|e\|$	V_O, Å^3
Stishovite	3.216 (3.865)[a]	2.702	−1.608 (−1.932)[a]	10.239
SiO_2-II	3.202 (3.903)[a]	2.777	−1.601 (−1.951)[a]	10.000
SiO_2-III	3.170 (4.020)[a]	2.950	−1.585 (−2.010)[a]	9.396

[a]In parentheses: spherically averaged Born dynamical charges.

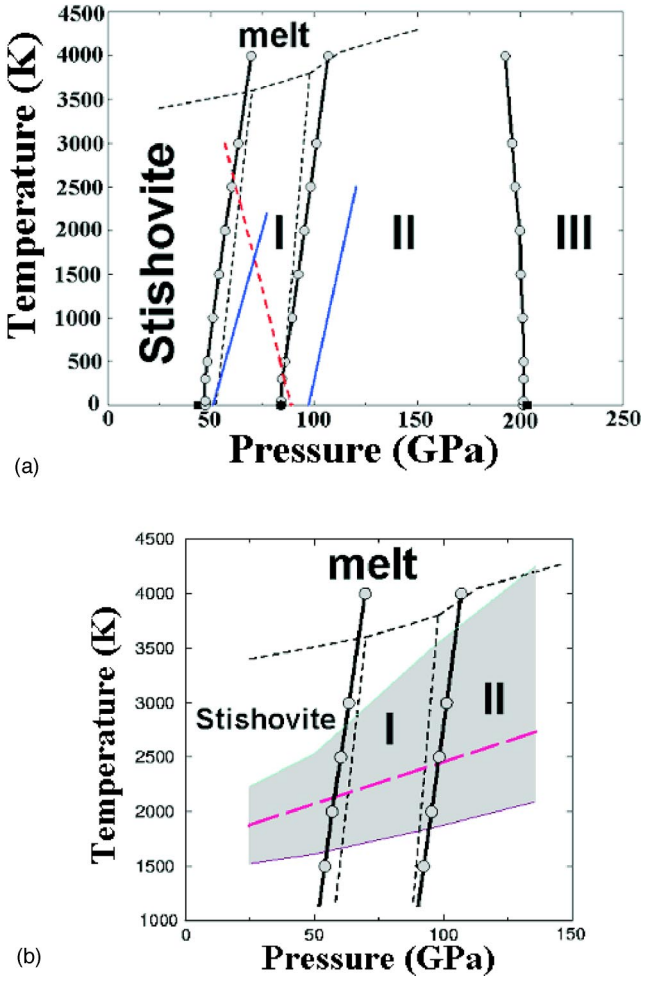

FIG. 3. (Color online) Calculated phase diagram of SiO_2. (a) Comparison with experimental results [solid blue (Ref. 34), long-dashed red (Ref. 13), dashed black lines (Ref. 33)]. (b) Search for seismic discontinuities. Dashed pink line: mantle adiabat, shaded area: possible temperature variations from Ref. 37. Solid black lines with circles: this work, dashed black lines: Ref. 33.

III. PHASE DIAGRAM

The calculated phase diagram (Fig. 3) is very simple and agrees remarkably well with the diagram sketched by Akins and Ahrens[33] on the basis of their shock compression data and reasonably well with (Ref. 34). Recent theoretical work[35] also gives similar results. However, experiments of Ref. 13 do not agree with our results for the (SiO_2-I)-(SiO_2

-II) equilibrium line. In Ref. 13, SiO_2-II was obtained not by compression of SiO_2-I, but by pressurising cristobalite structure in the region of its metastability and therefore what the authors of Ref. 13 observed was probably a thermally activated metastable transition cristobalite-(SiO_2-II), facilitated by temperature and therefore having a negative Clapeyron slope. This is not too surprising, given the multitude of known metastable phases and transitions in SiO_2 (see, e.g., Refs. 7 and 14).

There has been some experimental evidence[36] that at pressures 62–100 GPa and temperatures 1900–3200 K, $MgSiO_3$ perovskite breaks down into the mixture of oxides, MgO and post-stishovite phase of SiO_2 identified[36] as SiO_2-II. An implication of these results would be that SiO_2-II is a major mineral phase of the lower mantle. From our phase diagram (Fig. 3) we see, however, that most of the P,T conditions indicated in Ref. 36 correspond to stability of SiO_2-I. Moreover, most experiments (e.g., Ref. 38 and 39) and recent *ab initio* calculations[26] show that $MgSiO_3$ perovskite does not decompose into $MgO+SiO_2$ at lower mantle conditions.

This implies that pure SiO_2 phases in the lower mantle can exist only in SiO_2-rich regions associated with subduction of relatively cold lithospheric slabs [in the rest of the lower mantle $MgO/SiO_2>1$, and any free SiO_2 would react with MgO (Ref. 26)]. Using our calculated phase diagram one can predict the depths of seismic discontinuities that could occur due to phase transitions of SiO_2 inside the Earth's mantle. If SiO_2 phases were abundant in areas of subduction, one would expect two seismic discontinuities [Fig. 3(b)], one between 1350 km (55 GPa, 1630 K) and 1410 km (58 GPa, 2130 K) associated with the stishovite-(SiO_2-I) transition and the other one between 2145 km (94 GPa, 1830 K) and 2210 km (90 GPa, 2440 K) due to the (SiO_2-I)-(SiO_2-II) transition. The LDA typicaly underestimates transition pressures by several GPa, so in reality these phase transitions could occur 100–200 km deeper. Still, these depths (~1500 and ~2300 km) do not correspond to any observed seismic discontinuities. Reference 35 relates the (SiO_2-I)-(SiO_2-II) transition to the so-called D'' discontinuity at 2700 km,[40] but this is inconsistent with present results: the depth of transition does not agree with our results and the transition itself, involving only minor changes in shear wave velocity, cannot explain the observed large shear wave discontinuity. In addition, the (SiO_2-I)-(SiO_2-II) transition is associated with a large decrease in elastic anisotropy[41] that is inconsistent with large seismic anisotropy below 2700 km.[42] In fact, seismic velocity jumps due to the (SiO_2-I)-(SiO_2-II) transition are small [~1% in pure SiO_2 Ref. 41] and for all realistic compositions (amount of SiO_2 phases below 30 vol. %) it would be undetectible with current seismological techniques. However, the effect of the stishovite-(SiO_2-I) transition on seismic velocities is much larger [~60% for shear waves (Ref. 41)] and should be observable if any significant amount (>2 vol. %) of SiO_2 phases were present in the lower mantle. Since no discontinuity is known at 1500 km, we conclude SiO_2 polymorphs do not exist in significant amounts in any extended regions of the Earth's lower mantle.

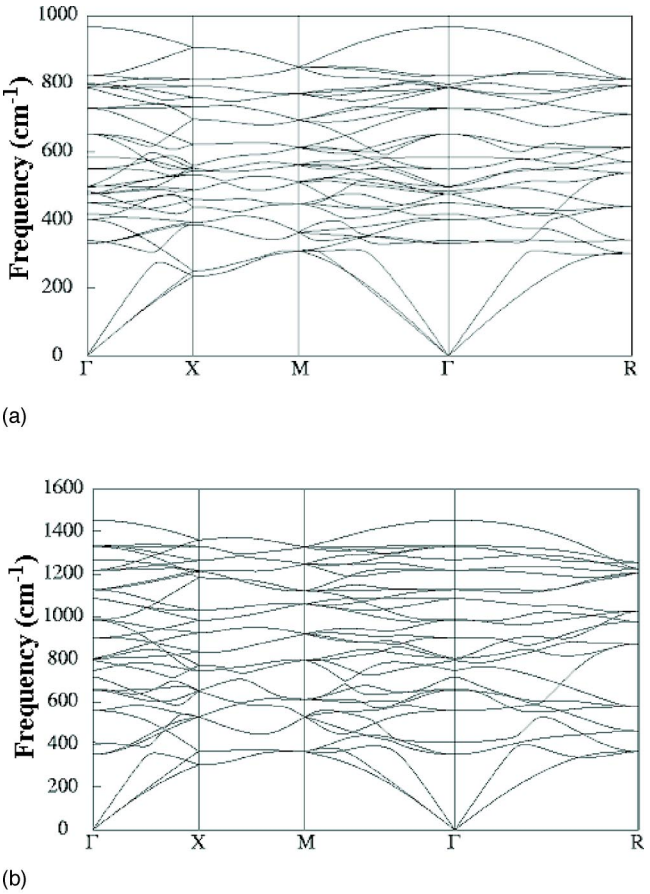

FIG. 4. Phonon dispersion curves for SiO_2-III at $P=0$, showing no soft modes.

IV. PYRITE-TYPE PHASE (SiO_2-III) AND BREAKDOWN OF CLOSE PACKING

It is known that stishovite and SiO_2-II possess remarkably high hardnesses,[43] but SiO_2-III may be even harder, since this cubic phase has a significantly higher bulk modulus (at zero pressure 344±3 GPa, as found from the elastic constants and the equation of state, Table II). We find that SiO_2-III is dynamically and mechanically stable at least in the range 0–260 GPa (see Fig. 4), and therefore could be decompressed to ambient conditions.

SiO_2-III is very interesting from the crystal-chemical point of view: its structure is unusual for an oxide and suggests (by analogy with pyrite-type chalcogenides) that there could be O-O bonds. Structures of stishovite, SiO_2-I, and SiO_2-II are based on the increasingly regular hexagonal close packing of O atoms. The question is why SiO_2-III, in spite of lack of anion close packing, is much denser than these phases and becomes more stable at extreme pressures. We remind the reader that density is a crucial factor for high-pressure stability.

First, we argue that there are no O-O bonds in the structure. The structure of SiO_2-III has only two independent variables—the oxygen coordinate x_O and the unit cell parameter. At $x_O \approx 0.10-0.15$ one has the molecular CO_2-type structure, at $x_O=0.25$ the fluorite structure. By increasing x_O to above 0.345 one arrives at the normal pyrite structure with

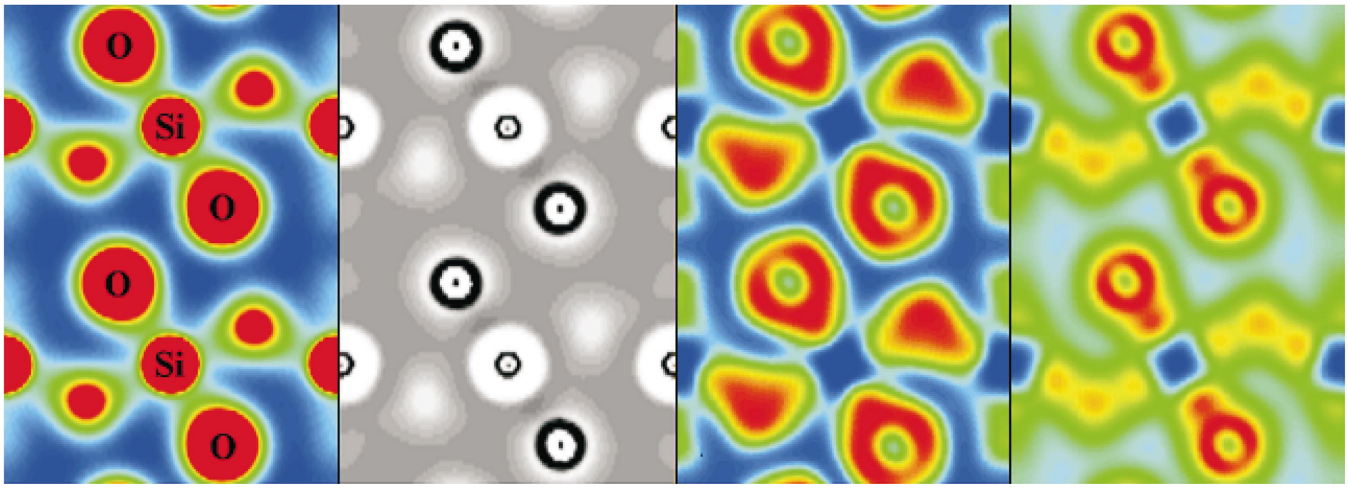

FIG. 5. SiO_2-III: distributions of (from left to right): total electron density (values from 0.11 to 1.5e Å^{-3} shown), its Laplacian (−20 to +20e Å^{-5}), electron localization function (0 to 0.87), localized orbital locator (0.02 to 0.63). LDA calculations at $P=0$. The Laplacian is everywhere positive, except thin spherical shells close to nuclei. The electron localization function and localized orbital locator were computed [with VASP code (Ref. 44)] only for valence electrons; regions of localization (values >0.5) are shown in red.

distinct O-O "dumbells," at $x_O=0.345$ the "dumbell" O-O distance becomes equal to six other O-O distances, and at $x_O<0.345$ "dumbells" dissociate. Although SiO_2-III is just on the border ($x_O=0.344$ at $P=0$, 0.350 at 260 GPa), topological analysis shows a (3,−1) critical point in the middle of each O-O "dumbell" in this structure at all pressures, as in typical pyrite structures. However, this is not a bonding interaction: the O-O interatomic distance (2.385 Å at $P=0$ and 2.043 Å at 260 GPa) in SiO_2-III is much longer than the usual distances of 1.4–1.5 Å of peroxide bonds and more similar to nonbonding O-O distances in ionic oxides (>2.2 Å at $P=0$). Although there is a (3,−1) critical point between these atoms, the corresponding electron density is low (0.22e Å^{-3}) and $\nabla^2\rho$ is positive (3.45e Å^{-5}) and suggestive of a closed-shell interaction, probably repulsive between like atoms. Figure 5 shows maps of the total electron density, its Laplacian, the electron localization function, and localized orbital locator in the (110) plane of SiO_2-III. These maps indicate mixed ionic-covalent character of Si—O bonds, but no covalent bonding between the O atoms. In particular, between these atoms one sees no peak in the electron localization function or the localized orbital locator, and $\nabla^2\rho$ is positive. It is clear from Fig. 5 that oxygen atoms are highly aspherical in SiO_2-III.

For the breakdown of close packing under pressure, two mechanisms are well known: (1) increase of the cation/anion size ratio with pressure that leads to high (>6) coordination numbers incompatible with close packing, and (2) complex electronic reorganisation within the solid.[45] Neither applies to our case. As discussed in Sec. II, in all considered structures Si atoms are 6-coordinated, and there are no major differences in bonding between SiO_2-III and other silica phases.

In the present case, the high density of SiO_2-III and its stability at high pressure are explained by the asphericity of oxygen atoms in its structure (visible in Fig. 5): indeed, packing of aspherical atoms can be denser than close packing of hard spheres. The asphericity itself is due to partial covalency of Si—O bonds and steric deformations of atoms in the structure. According to our *ab initio* results, SiO_2-III is 5% denser than close-packed SiO_2-II at zero pressure, whereas the hard-sphere model incorrectly predicts 19% lower density.

Among simple models alternative to the traditional "hard-sphere" thinking, there are "deformable sphere" models (e.g., pair potential models,[46] which correctly predict SiO_2-III to be denser than SiO_2-II) and "bond network" models that focus on bond lengths (which show only modest variations in crystals) rather than on radii of atoms (which are allowed to be aspherical). The best of the latter models, Brown's bond

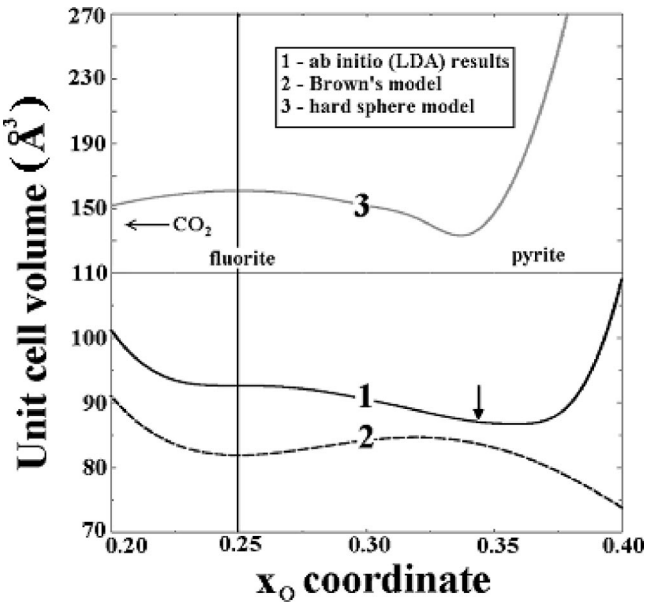

FIG. 6. Unit cell volume of SiO_2-III as a function of oxygen coordinate x_O. Vertical arrow: minimum-energy value of x_O. Line 1 was obtained by total energy energy minimization with constrained x_O. Line 3 used the hard-sphere radius of 1.36 Å. Note the change of scale at the volume of 110 Å^3.

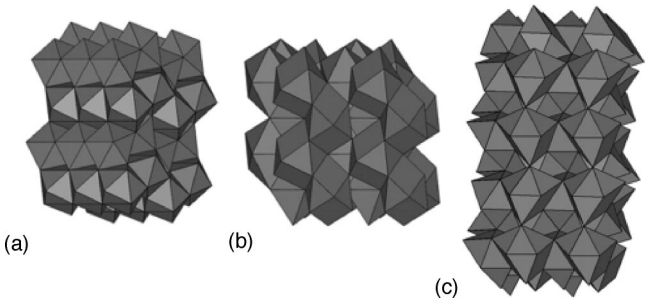

FIG. 7. Structures of (a) cotunnite-type, (b) baddeleyite-type, (c) OI-type phases of SiO_2.

valence model,[47] allows one to predict bond lengths for each topology by solving bond-valence balance equations. Within this model, SiO_2-III is correctly predicted to be 6% denser than undistorted close-packed polymorphs. The dramatic failure of the hard-sphere model and success of even the simplest models that are able to account for deformability of atoms leads us to conclude that deformability of atoms is a key factor in the breakdown of close packing under pressure. There can, in principle, be many structures that are denser than their close-packed counterparts; in these structures, atoms are not spherical and experience "squeezing" at short distances (e.g., in SiO_2-III O atoms are "squeezed" at short O-O contacts). Though energetically costly, this may enable greater density and, thus, stability at high pressure.

Figure 6 shows an *ab initio* zero-pressure unit cell volume of SiO_2-III as a function of x_O (line 1), in comparison with two simple models: Brown's model (line 2) and hard-sphere model (line 3). Even the shape of this line cannot be reproduced by a simple hard-sphere model (line 3). Brown's model is rather successful, its difference from *ab initio* results being mainly due to steric O-O repulsion,[47] which is greatest in the fluorite structure ($x_O=0.25$) and $x_O>0.375$ (pyrite structure with very close O-O contacts) and smallest at $x_O\approx 0.34$ (*cf.* our *ab initio* structure with $x_O=0.344$). Thus, the structure of SiO_2-III found in *ab initio* calculations combines high density and only modest anion-anion repulsion.

V. POST-PYRITE PHASES

For the reasons discussed above, SiO_2-III appears to be a remarkably stable phase. As possible post-pyrite phases, we have considered the baddeleyite (space group $P2_1/c$, 12 atoms per unit cell), cotunnite (*Pnma*, 12 atoms per cell), and the OI structure (*Pbca*, 24 atoms per cell) recently found in TiO_2;[48] these structures are shown in Fig. 7. For these phases, the Brillouin zone was sampled by $4\times4\times4$, $4\times8\times4$, and $2\times4\times4$, respectively; all other computational settings are the same as described in Sec. II. At zero K, only the cotunnite structure has a region of stability—it becomes more stable than SiO_2-III above 750 GPa (Fig. 8). In this non-close-packed structure Si atoms are in the ninefold coordination, which is incompatible with close packing. The

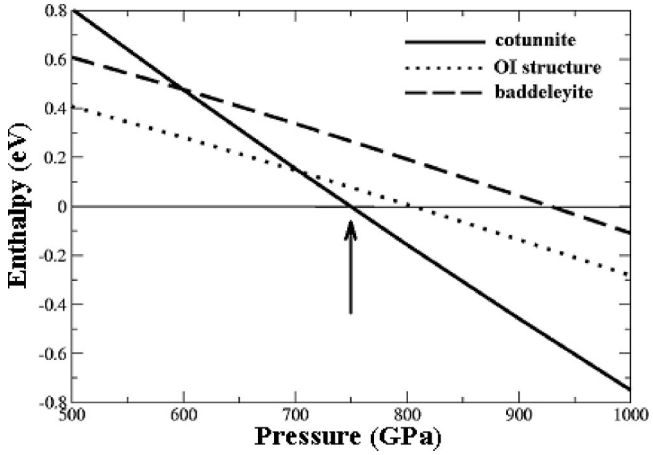

FIG. 8. Enthalpies (relative to SiO_2-III, per f.u.) of post-pyrite phases of SiO_2. Phase transition to the cotunnite structure is marked by an arrow.

OI-type structure is only marginally less stable at zero K, and cannot be ruled out as a possible stable phase at high temperatures and pressures ~700–800 GPa.

VI. SUMMARY

Silica (SiO_2) undergoes a series of post-stishovite structural phase transitions: first into a $CaCl_2$-type phase (~50 GPa), then into an α-PbO_2-type (~90 GPa), pyrite-type (~200 GPa), and cotunnite-type (750 GPa) phases. Using density-functional perturbation theory, we have calculated the high-pressure phase diagram of SiO_2. We conclude that it is unlikely that SiO_2 polymorphs exist in significant amounts in any large portion of the Earth's lower mantle. Pressure-induced breakdown of close packing in SiO_2, predicted to occur at 200 GPa, has been examined in detail and explained by deformability of atoms enabling high density for non-close-packed structures: for a system of deformable ions, non-close-packed structures may turn out to be denser and more stable at high pressure. This mechanism for pressure-induced breakdown of close packing is expected to be very common. One of further examples is provided by Al_2O_3, where close-packed corundum phase transforms at ~90 GPa into a non-close-packed Rh_2O_3(II) structure (Ref. 49, and references therein) without changes in the electronic structure or atomic coordination numbers. We expect that appearance of non-close-packed phases at high pressure should be a general feature of many materials, including silicates and oxides.

ACKNOWLEDGMENTS

We thank S. Ono for discussions, CSCS (Manno, Switzerland) and CSAR (U.K.) for access to supercomputers and ETH Zurich for funding.

*E-mail address: a.oganov@mat.ethz.ch

[1] S. M. Stishov and S. V. Popova, Geokhimiya **10**, 837 (1961).

[2] R. J. Angel, N. L. Ross, F. Seifert, and T. F. Fliervoet, Nature (London) **384**, 441 (1996).

[3] A. R. Oganov, G. D. Price, and J. P. Brodholt, Acta Crystallogr., Sect. A: Found. Crystallogr. **57**, 548 (2001).

[4] R. E. Cohen, in *High Pressure Research in Mineral Physics: Application to Earth and Planetary Science*, edited by M. H. Manghnani and Y. Syono (AGU, Washington, D.C., 1992).

[5] K. J. Kingma, R. E. Cohen, R. J. Hemley, and H.-K. Mao, Nature (London) **374**, 243 (1995).

[6] B. B. Karki, M. C. Warren, L. Stixrude, G. J. Ackland, and J. Crain, Phys. Rev. B **55**, 3465 (1997); **56**, 2884(E) (1997).

[7] D. M. Teter, R. J. Hemley, G. Kresse, and J. Hafner, Phys. Rev. Lett. **80**, 2145 (1998).

[8] L. S. Dubrovinsky, S. K. Saxena, P. Lazor, R. Ahuja, O. Eriksson, J. M. Wills, and B. Johansson, Nature (London) **388**, 362 (1997).

[9] D. Andrault, G. Fiquet, F. Guyot, and M. Hanfland, Science **282**, 720 (1998).

[10] S. R. Shieh, T. S. Duffy, and B. Li, Phys. Rev. Lett. **89**, 255507 (2002).

[11] R. J. Hemley, J. Shu, M. A. Carpenter, J. Hu, H.-K. Mao, and K. J. Kingma, Solid State Commun. **114**, 527 (2000).

[12] M. A. Carpenter, R. J. Hemley, and H. K. Mao, J. Geophys. Res. **105**, 10807 (2000); for a review on lower-mantle discontinuities see L. Vinnik, M. Kato, and H. Kawakatsu, Geophys. J. Int. **147**, 41 (2001).

[13] L. S. Dubrovinsky, N. A. Dubrovinskaya, S. K. Saxena, F. Tutti, S. Rekhi, T. LeBihan, G. Shen, and J. Hu, Chem. Phys. Lett. **333**, 264 (2001).

[14] V. P. Prakapenka, G. Shen, L. S. Dubrovinsky, M. L. Rivers, and S. R. Sutton, J. Phys. Chem. Solids **65**, 1537 (2004).

[15] J. Haines, J. M. Leger, and O. Schulte, Science **271**, 629 (1996).

[16] S. Ono, T. Tsuchiya, K. Hirose, and Y. Ohishi, Phys. Rev. B **68**, 014103 (2003).

[17] S. Baroni, S. de Gironcoli, A. Dal Corso, and P. Gianozzi, Rev. Mod. Phys. **73**, 515 (2001).

[18] J. P. Perdew and Y. Wang, Phys. Rev. B **45**, 13 244 (1992). Our LDA static pressures for the stishovite/SiO_2-I, SiO_2-I/SiO_2-II, and SiO_2-II/SiO_2-III transitions are 44, 84, and 204 GPa, respectively. This is similar to previous theoretical and experimental values. Using the all-electron PAW method [G. Kresse and D. Joubert, *ibid.* **59**, 1758 (1999); P. E. Blöchl, *ibid.* **50**, 17 953 (1994)], GGA [Y. Wang and J. P. Perdew, *ibid.* **44**, 13 298 (1991)], and the VASP code (Ref. 44) we get values of 55, 97, and 217 GPa for the stishovite/SiO_2-I, SiO_2-I/SiO_2-II, and SiO_2-II/SiO_2-III transitions, respectively.

[19] X. Gonze, J.-M. Beuken, R. Caracas, F. Detraux, M. Fuchs, G.-M. Rignanese, L. Sindic, M. Verstraete, G. Zerah, F. Jollet, M. Torrent, A. Roy, M. Mikami, Ph. Ghosez, J.-Y. Raty, and D. C. Allan, Comput. Mater. Sci. **25**, 478 (2002). ABINIT code is a common project of the Université Catholique de Louvain, Corning Inc., and other contributors (URL: //www.abinit.org). ABINIT relies on an efficient fast Fourier transform algorithm [S. Goedecker, SIAM J. Sci. Comput. (USA) **18**, 1605 (1997)] for the conversion of wave functions between real and reciprocal space, on the adaptation to a fixed potential of the band-by-band conjugate gradient method [M. C. Payne, M. P. Teter, D. C. Allan, T. A. Arias, and J. D. Joannopoulos, Rev. Mod. Phys. **64**, 1045 (1992)] and on a potential-based conjugate-gradient algorithm for the determination of the self-consistent potential [X. Gonze, Phys. Rev. B **54**, 4383 (1996)]. Technical details on the computation of responses to atomic displacements and homogeneous electric fields can be found in [X. Gonze, *ibid.* **55**, 10 337 (1997)], and the subsequent computation of dynamical matrices, Born effective charges, dielectric permittivity tensors, and interatomic force constants was described in Ref. 22.

[20] N. Troullier and J. L. Martins, Phys. Rev. B **43**, 1993 (1991).

[21] S. G. Louie, S. Froyen, and M. L. Cohen, Phys. Rev. B **26**, 1738 (1982).

[22] X. Gonze and C. Lee, Phys. Rev. B **55**, 10 355 (1997).

[23] A. R. Oganov, M. J. Gillan, and G. D. Price, J. Chem. Phys. **118**, 10 174 (2003).

[24] R. A. Robie and B. S. Hemingway, *Thermodynamic properties of minerals and related substances at 289.15 K and 1 bar (*10^5 *Pascals) pressure and at higher temperatures*U.S. Geological Survey Bulletin 2131, (1995). We recalculated C_V from the reported C_P.

[25] M. Akaogi, H. Yusa, K. Shiraishi, and T. Suzuki, J. Geophys. Res. **100**, 22337 (1995). We recalculated C_V from the reported C_P.

[26] A. R. Oganov and G. D. Price, J. Chem. Phys. (to be published).

[27] M. Akaogi and E. Ito, Geophys. Res. Lett. **20**, 105 (1993). We recalculated C_V from the reported C_P.

[28] P. Vinet, J. H. Rose, J. Ferrante, and J. R. Smith, J. Phys.: Condens. Matter **1**, 1941 (1989).

[29] A. R. Oganov and S. Ono, Nature (London) **430**, 445 (2004).

[30] R. F. W. Bader, *Atoms in Molecules. A Quantum Theory* (Oxford University Press, Oxford, 1990).

[31] A. D. Becke and K. E. Edgecombe, J. Chem. Phys. **92**, 5397 (1990).

[32] H. L. Schmider and A. D. Becke, J. Mol. Struct. **527**, 51 (2000).

[33] J. A. Akins and T. J. Ahrens, Geophys. Res. Lett. **29**, 1394 (2002).

[34] S. Ono, K. Hirose, M. Murakami, and M. Isshiki, Earth Planet. Sci. Lett. **197**, 187 (2002); M. Murakami, K. Hirose, S. Ono, and Y. Ohishi, Geophys. Res. Lett. **30**, 1207 (2003).

[35] T. Tsuchiya, R. Caracas, and J. Tsuchiya, Geophys. Res. Lett. **31**, L11610 (2004).

[36] S. K. Saxena L. S. Dubrovinsky, P. Lazor, Y. Cerenius, P. Häggkvist, M. Hanfland, and J. Hu, Science **274**, 1357 (1996).

[37] A. R. Oganov, J. P. Brodholt, and G. D. Price, Nature (London) **411**, 934 (2001); in *EMU Notes in Mineralogy*, edited by C. M. Gramaccioli (Eötvös University Press, Budapest, 2002), Vol. 4, pp. 83–170.

[38] S. H. Shim, T. S. Duffy, R. Jeanloz, and G. Shen, Geophys. Res. Lett. **31**, L10603 (2004).

[39] G. Serghiou, A. Zerr, and R. Boehler, Science **280**, 2093 (1998).

[40] T. Lay and D. V. Helmberger, Geophys. Res. Lett. **10**, 63 (1983).

[41] B. B. Karki, L. Stixrude, and J. Crain, Geophys. Res. Lett. **24**, 3269 (1997).

[42] M. Panning and B. Romanowicz, Science **303**, 351 (2004).

[43] N. A. Dubrovinskaia and L. S. Dubrovinsky, Mater. Chem. Phys. **68**, 77 (2001).

[44] G. Kresse and J. Furthmüller, Comput. Mater. Sci. **6**, 15 (1996); Phys. Rev. B **54**, 11 169 (1996).

[45] J. B. Neaton and N. W. Ashcroft, Nature (London) **400**, 141 (1999).

[46] A. R. Oganov, J. P. Brodholt, and G. D. Price, Phys. Earth Planet. Inter. **122**, 277 (2000).

[47] I. D. Brown, Acta Crystallogr., Sect. B: Struct. Sci. **48**, 553 (1992).

[48] N. A. Dubrovinskaia, L. S. Dubrovinsky, R. Ahuja, V. B. Prokopenko, V. Dmitriev, H.-P. Weber, J. M. Osorio-Guillen, and B. Johansson, Phys. Rev. Lett. **87**, 275501 (2001).

[49] J. F. Lin, O. Degtyareva, C. T. Prewitt, P. Dera, N. Sata, E. Gregoryanz, H.-K. Mao, and R. J. Hemley, Nat. Mater. **3**, 389 (2004).